Planetary and Space Science 117 (2015) 385–400

Contents lists available at ScienceDirect

Planetary and Space Science

journal homepage: www.elsevier.com/locate/pss

Geologic characteristics of the Luna 17/Lunokhod 1 and Chang'E-3/Yutu landing sites, Northwest Mare Imbrium of the Moon

A.T. Basilevsky [a,b,*], A.M. Abdrakhimov [a], J.W. Head [b], C.M. Pieters [b], Yunzhao Wu [c], Long Xiao [d]

[a] Vernadsky Institute, Russian Academy of Sciences, Moscow 119991, Russia
[b] Department of Earth, Environmental and Planetary Studies, Brown University, Providence, RI 02912, USA
[c] School of Geographic and Oceanographic Sciences, Nanjing University, Nanjing 210023, China
[d] Planetary Science Institute, China University of Geosciences, Wuhan 430074, China

ARTICLE INFO

Article history:
Received 26 May 2015
Received in revised form
11 August 2015
Accepted 12 August 2015
Available online 21 August 2015

Keywords:
Rover
mare
highland
regolith
crater
ejecta

ABSTRACT

We compared and assessed the results of measurements and observations by the Lunokhod 1 and Yutu rovers, both of which explored the northwestern part of Mare Imbrium. Both sites are within the distinctive Eratosthenian-aged lava flow geologic unit and our comparisons showed that the geologies of these exploration sites are very similar. As in the majority of other areas of the Moon, the dominant landforms in these sites are small impact craters, having various degrees of morphologic prominence and states of preservation, and rock fragments, mostly associated with the rims and interiors of fresh craters. The shape and the degree of preservation of the observed rock fragments in these two sites are similar. In both sites sporadic rock fragments were observed whose morphologies suggest that their source rocks had columnar jointing. Localization of these specific rocks on the rims of 450–470 m in diameter craters implies that the source rocks are at depths of 40–50 m. Regolith in the study areas is typically a few meters thick, but locally can be much thicker. The ground penetrating radar of the Yutu rover revealed the multilayer regolith structure, which is determined by superposition of crater ejecta; with some local variations, this type of the regolith stratigraphy should be typical of the majority of lunar mare sites. The physico-mechanical properties of the regolith in these two sites appear to be rather similar: the bearing capacity ranges from 0.04 to 1.44 kg/cm^2, with a modal value ~0.45 kg/cm^2, and the shear strength ranges from 0.02 to 0.1 kg/cm^2, with a modal value ~0.05 kg/cm^2. Both these factors decrease by a factor of 3–4 with an increase of surface slope from ~2 to 12°. The chemical composition of surface materials determined by the rover instruments at these two sites differ from those derived from the remote sensing data for the Eratosthenian-aged basalts on which the two sites are located. This could be partly due to low measurement accuracies, especially in the case of Lunokhod 1, but may also represent real variations in the composition of the surface materials compared to returned lunar samples. Difference in the spatial resolution of the in-situ and remote-sensing analyses should also be taken into account. Recommendations for future lunar rover missions are as follows: (1) to use ground penetrating radar and a robotic arm, and (2) to employ radial study tactics for impact crater documentation and analysis.

1. Introduction

This work is a part of a joint research project between Brown University, Providence, RI, USA, Nanjing University, Nanjing, China, China University of Geosciences, Wuhan, China, and the Vernadsky Institute, Moscow, Russia. Its goal is a study of the northwestern part of Mare Imbrium including Sinus Iridum, as well as Montes Jura, which is the adjacent part of the Imbrium basin rim. The formation of the Imbrium impact basin is considered to be the beginning of Imbrian epoch (Wilhelms, 1987), and its subsequent filling with basaltic lavas during the Imbrian and Eratosthenian time were important events in the geologic history of the Moon (Hiesinger et al. 2010). Within the study area are landing sites of the USSR Luna 17 lander, which on November 17, 1970, delivered to the lunar surface the Lunokhod 1 rover, and the Chinese Chang'E-3 spacecraft, which 43 years later on December 14, 2013,

* Corresponding author at: Vernadsky Institute, Russian Academy of Sciences, Moscow 119991, Russia. Tel.: +7 499 137 4995; fax: +7 495 938 2054.
E-mail address: atbas@geokhi.ru (A.T. Basilevsky).

http://dx.doi.org/10.1016/j.pss.2015.08.006

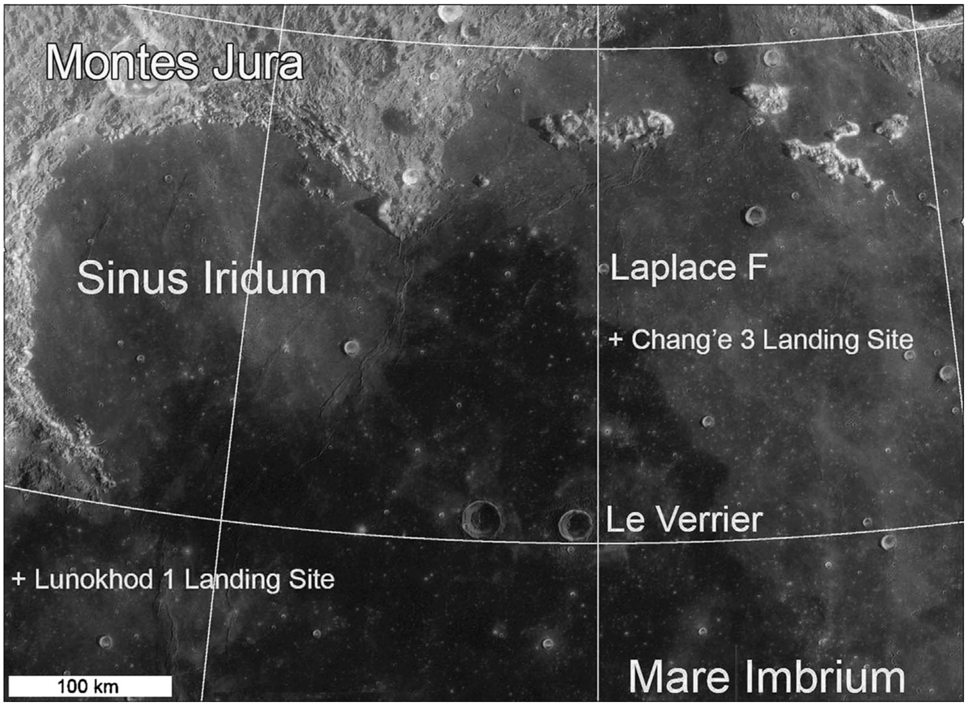

Fig. 1. A LRO WAC mosaic showing the northwestern part of Mare Imbrium and Sinus Iridum with locations of the Luna 17 and Chang'E-3 landing sites indicated. Courtesy of NASA/ASU/LPL. Both landing sites are located within the lower albedo Eratosthenian mare unit near its boundary with the slightly higher albedo and older Imbrian lava flows (Wu et al., 2015).

brought to this area of the Moon some 500 km to the northeast, the Yutu rover (Fig. 1).

In this project we analyzed different sets of data to characterize the landings and traverse regions and to intercompare them. The present paper is mostly based on analysis of the imagery and other data taken in-situ by the Lunokhod 1 and Yutu rovers, while the complementary paper (Wu et al., 2015) is based on analysis of the remote sensing data.

2. Lunokhod 1 area

The Luna 17 lander, with Lunokhod 1 onboard, landed in the northwestern part of Mare Imbrium ~75 km SE of Promontorium Heraclides, which is a part of Montes Jura. According to analysis of remote sensing data, the landing site is within the Eratosthenian lava unit (Schaber, 1969, 1973; Hiesinger et al., 2010; Qiao et al., 2014) near the boundary with Imbrian-aged lavas (Wu et al., 2015; Zhang et al., 2015). The typical landscape of the Lunokhod 1 study area is shown in Fig. 2.

The Luna 17 landing site coordinates are 38.24°N, 35.00°W, and the coordinates of the ending position of Lunokhod 1 are 38.32°N, 35.01°W (determined from the map of Shingareva et al., 2012). The total length of the Lunokhod 1 route was 9436 m (Fig. 3). The last communication session with Lunokhod 1 was on September 30, 1971 on the eve of lunar night after which Lunokhod 1 did not respond to control center commands (Ivanov et al., 1978).

Lunokhod 1 is an eight-wheel rover with a mass of 756 kg (Anisov et al., 1971). Its wheel track width was 20 cm in the soil, and when the rover tracks are seen in panoramas their width is a convenient tool to measure sizes and distances in the close vicinity of the rover. Lunokhod 1 explored the lunar surface using the following instruments: (1) four panoramic cameras, (2) Penetrometer PROP (PRibor Otsenki Prokhodimosti=Instrument to measure trafficability) to measure physico-mechanical properties of the surface material, and (3) X-ray fluorescence spectrometer RIFMA (Roentgen Isotopic Fluorescent Method of Analysis) to measure the elemental composition of the surface material. The rover also had an X-ray telescope and cosmic ray detectors to measure the radiation environment, and a laser retroreflector to measure with high precision the Earth–Moon distances by laser ranging from observatories on Earth (Fig. 4).

A digital terrain model (DTM) was produced for this area based on the analysis of LRO NAC image stereopairs (Karachevtseva et al., 2013). It was found that the altitude range in the area is ~50 m, while for the entire Lunokhod 1 route the altitude range was not more than ~25 m and the slopes, measured at a baseline of the rover wheel separation distance (~2 m), are typically less than ~10°. The rover first moved to the south. It then turned back to the landing site and continued its way to the north, making a rather large loop SW of crater Borya (Fig. 3).

Fig. 5 shows the Luna 17 lander with the rover wheel offramps and the rover wheel tracks. The images were taken late in January 1971 when the rover returned back to the lander.

2.1. Craters

The landscape-forming features in the area of landing site and its vicinity are mostly impact craters of meters, tens and hundreds of meters in diameter scale (Fig. 6).

In Fig. 6, craters several meters in diameter, with various degrees of morphological prominence, are observed and the centimeter- to decimeter-size rock fragments are seen as well. On the basis of their degree of morphological prominence, craters are classified into three main morphologic classes (A, B and C), and two intermediate classes (AB and BC), first suggested by Florensky and Taborko (1972) (Fig. 7).

Craters of classes A, AB, B, BC and C typically comprise 0.5–1, 2–3, 15–20, ~30 and ~50% of the total population of small craters, correspondingly (Florensky et al., 1971, 1972, 1978; Basilevsky 1976). They represent the evolutionary sequence from newly-formed craters of class A to strongly degraded craters of class C. The

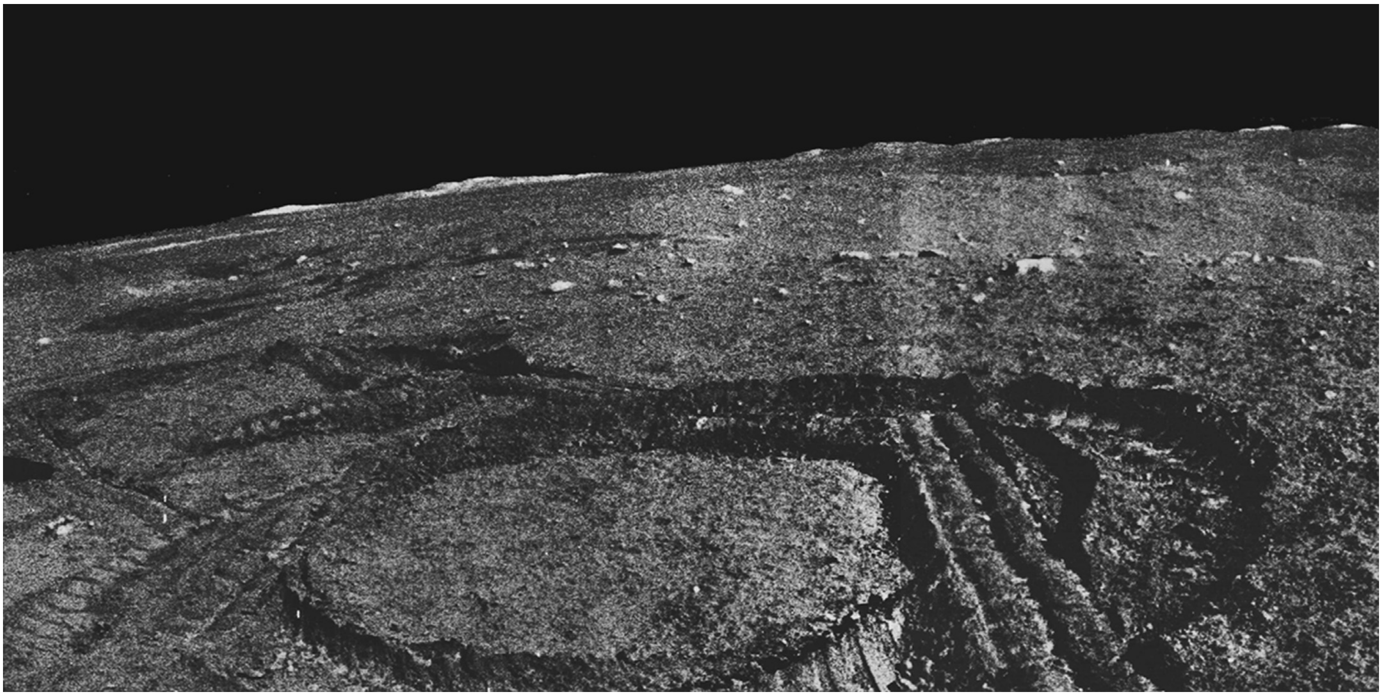

Fig. 2. Landscape at the Lunokhod 1 study area with the mountains of Promontorium Heraclides on the horizon. The rover tracks are seen in the lower part of the image and in the upper right is seen part of a relatively large crater with rock fragments outlining its rim. Part of TV panorama L1_D11_S01_P01. Here and in further references, the meaning of the panorama numbering system is: L1–Lunokhod 1, D11–number of working day (lunation), S01–number of working session during this day, P01–number of panorama taken at this session.

morphologic prominence of small lunar craters depends on their age and size: craters of smaller size degrade from the class A to class C faster than craters of larger size. Estimates of the potential lifetimes of small lunar craters (Basilevsky, 1974, 1976) were made by considering the intersection of craters of different sizes (and representing different morphologic classes) in comparison with morphologic analysis of several craters at the Apollo landing sites, for which absolute ages of formation were found from isotopic studies of the returned samples. In these studies, a crater lifetime was interpreted as the time during which a crater in the process of its degradation could still be visually identified. In the recent work of Basilevsky et al. (2014) on the morphometry of small craters in the areas traversed by Lunokhod 1 and 2, it was found that the visual identification of craters is typically possible if the crater depth/diameter ratio is larger than ~0.03.

It was found that for craters smaller than ~150 m in diameter, the potential crater lifetime T depends on the crater diameter D, as $T=2.5\ D$, where T is in millions of years (Ma) and D is in meters. For craters larger than ~150 m in diameter, the $T(D)$ dependence was found to be T (Ma)$=8D$ (m)–900 (Ma). So, for example, for craters having $D=100$ m, their potential lifetime will be ~250 Ma. Craters of this size belonging to class A and thus representing the first 0.5–1% of the crater evolution are not older than 1.2–2.5 Ma, and so on. The majority of craters seen on Lunokhod 1 panoramas are not larger than 5–10 m in diameter so they are not older than 12–25 Ma, while the largest crater in this area, Borya, (morphologic class B, $D=470$ m) was formed between 100 and 500 Ma ago (Abdrakhimov et al., 2014). As discussed by Basilevsky (1974), the accuracy of this method is ~30% of the determined age. To improve upon this estimate and technique, new sample return missions to the Moon are necessary.

2.2. Rock fragments

The rock fragments in the Lunokhod 1 study area (and in majority of other areas of the Moon as well) are mostly associated with rims and internal slopes of rather large (tens and hundreds meters in diameter) craters which, during the impact event, penetrated through the regolith layer to the rocky substrate (e.g., Morris and Shoemaker, 1968; Florensky et al., 1971, 1977; Schultz, 1976) (Fig. 8).

It is seen in Fig. 8a that 0.5–1 m-sized rocks on the rim of Borya Crater (comprising a cluster to the right center of the image) have a subdued morphology that implies their relatively long exposure on the lunar surface (more than tens of millions years according to Basilevsky et al. (2013)). This agrees with the observed absence of 2–5 m sized boulders on the rim of Borya Crater in LRO NAC image M150749234LC. This 470-m crater belongs to morphologic class B and using the technique of Basilevsky (1976) allows one to estimate its age as approximately 150–200 Ma (Abdrakhimov et al., 2014). Rocks seen in Fig. 8b are on the internal slope of the same crater, Borya. They are sharp-edged and angular suggesting a shorter time of surface exposure probably due to evolution of the regolith layer on the rather steep inner slope of this crater by the downslope material movement and due to excavation by the new-formed smaller crater (e.g., Schultz, 1976; Basilevsky et al., 2014).

Rocks seen on the images differ in primary shape and degree of degradation (Fig. 9) and can be classified according to these parameters (e.g., Florensky et al., 1978).

The primary shape of these rocks depends on the character of jointing of the source rock. Columnar jointing, typical for basalts, does not necessarily lead to only prismatic shapes. All rock shapes observed in Lunokhod 1 area could be formed by fragmentation of rocks with columnar jointing (see also, http://marlimillerphoto.com/Ig-84.html) and especially if the formation of rock fragments from the rock basement occurs under such dynamic conditions as high-velocity impacts.

A rock fragment whose shape suggests that the source rock could have been characterized by columnar jointing is shown in Fig. 10.

It is seen in Fig. 10 that the rover had partly driven on the ~30 × 50 cm rock fragment that led to separation along a part of the rock (arrow) parallel to the rock jointing planes. This location

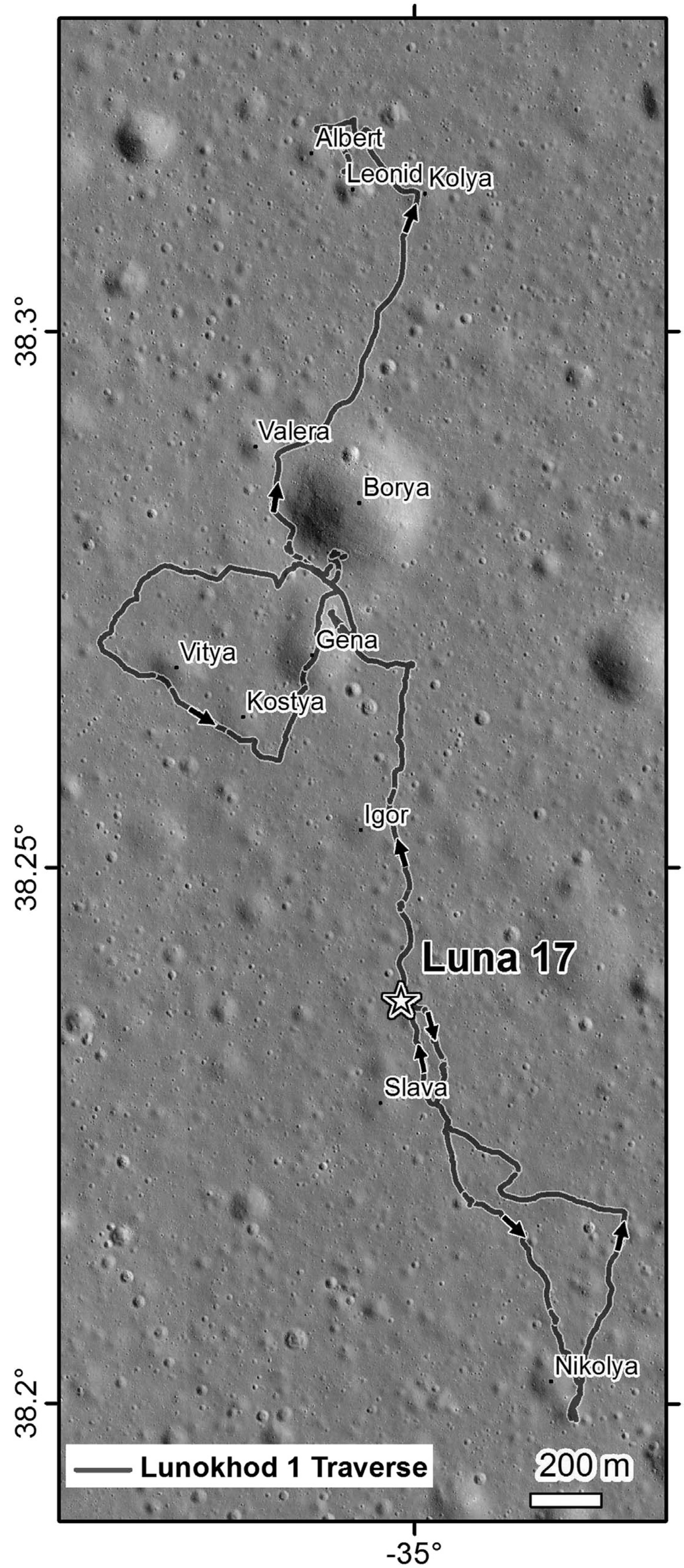

Fig. 3. Lunokhod 1 traverse on the background of LRO WAC mosaic. Courtesy of NASA/ASU/LPL. Crater names on the map are the first names of the Lunokhod crew members and leader of the science team Boris Nepoklonov (Borya) (http://planetarynames.wr.usgs.gov/).

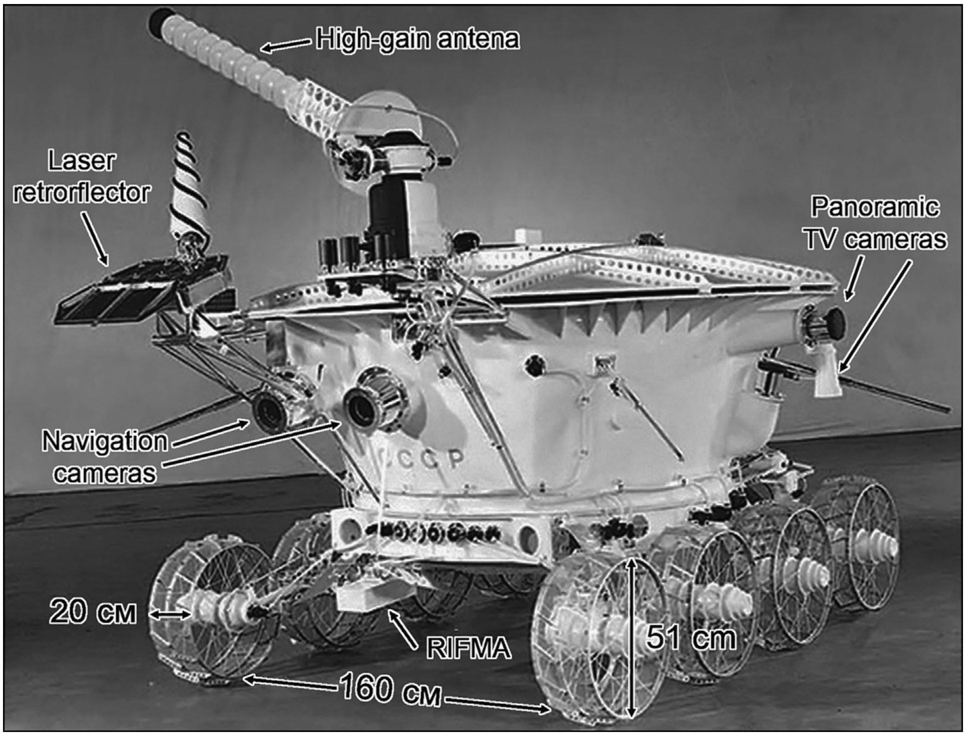

Fig. 4. Lunokhod 1 mockup with major sizes and instruments shown. Courtesy of Lavochkin Association/Roskosmos.

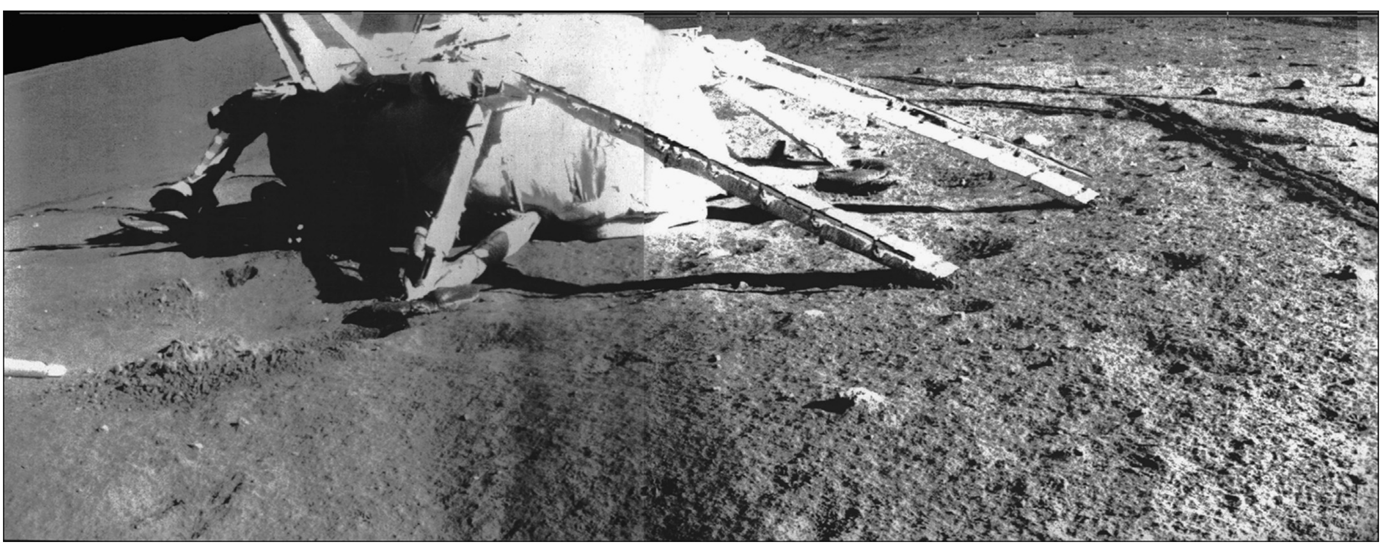

Fig. 5. The lander seen by the TV panoramic camera of the rover. The camera is looking to the south. The width between the rover wheels base is 160 cm and the wheel width is 20 cm. Portions of panoramas L1_D03_S07_P19 and L1_D03_S07_P14, correspondingly.

is on the WSW rimcrest of the 470-m Borya Crater, and this implies that the depth of excavation of this crater is ~40–50 m (Melosh, 1989, formula 5.5.4). Typically the rimcrest is the place where the deepest part of the target material is deposited, and thus the rock with columnar jointing probably came from this ~40–50 m depth. Its morphologic freshness suggests that the majority of the time since the formation of Borya Crater (150–200 Ma ago, see above) it was buried in the subsurface and only recently exposed, probably by a small crater-forming event.

2.3. Regolith

Regolith surfaces were observed along all traverse of Lunokhod 1; no outcrops of rocky basement were seen. The presence of rock fragments in ejecta of morphologically fresh craters which, at the time of their formation, penetrated through the regolith to the rocky basement, permitted the estimation of the typical thickness of regolith layer in the Lunokhod 1 area to be ~4–6 m (Florensky et al., 1978). On the rims of the largest fresh craters (200–500 m in diameter) the regolith thickness may reach 10–15 m: sum of pre-crater regolith thicknesses and thicknesses of the crater ejecta, for the latter see also McGetchin et al. (1973), formula 3; Basilevsky et al. (1983), formula II.34). On the floors of the largest degraded craters (classes BC and C) the regolith thickness may reach a few tens of meters: filling of fresh craters ($H/D \approx 1/5$) with ejecta from other craters to reach the degradation stage BC-C ($H/D \leq 1/10$). On the rims and slopes of relatively large fresh craters, the surface of the regolith is covered with rock fragments. In other geomorphologic situations,

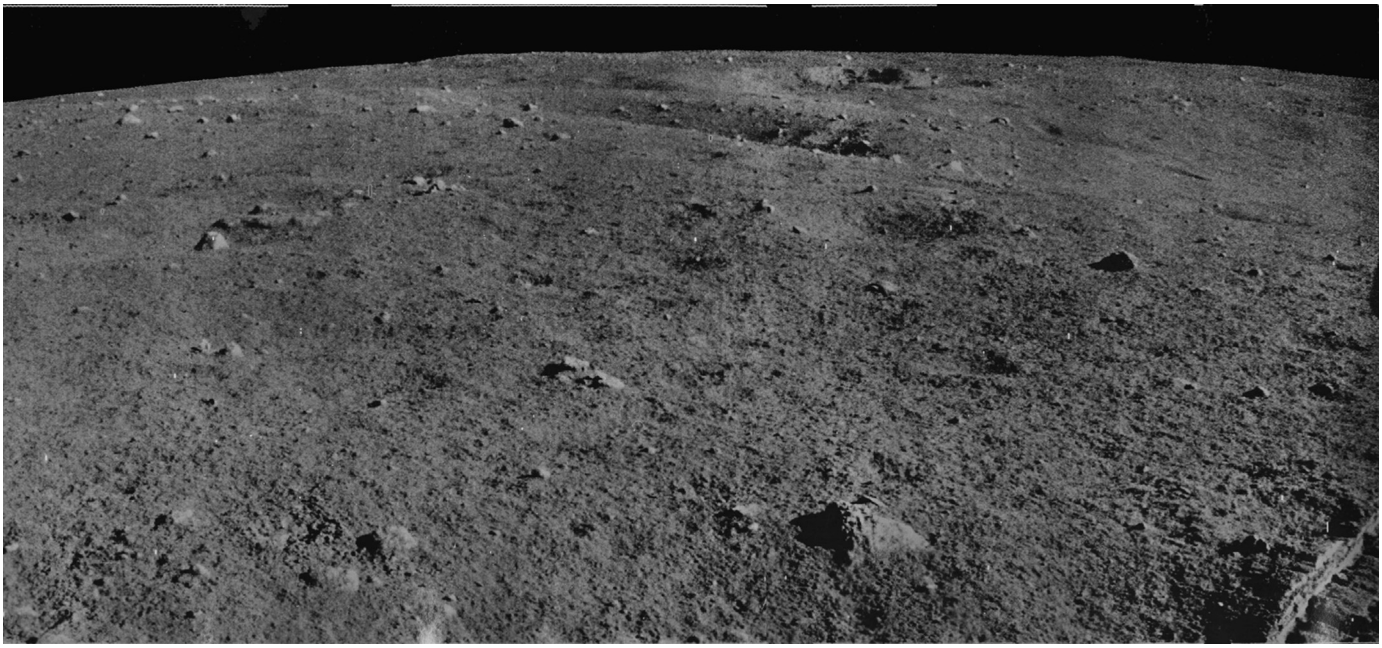

Fig. 6. Typical landscape in the Lunokhod 1 study area. Portion of panorama L1_D09_S05_P10.

when the surface is free of rock fragments, it typically has a smooth to cloddy texture, and containing gravel-size particles. Fig. 11 shows the surfaces of undisturbed regolith and the results of deformation of the regolith by the Lunokhod turning in place.

It is seen in Fig. 11b that clockwise displacement of regolith material by the rotating and turning wheel caused the newly-formed surface to be smooth due to compaction and shear. Fig. 11c also shows the result of clockwise material displacement, leading to material piling up, with the surface consisting of centimeter-sized clods and probably rock fragments. This figure demonstrates the cohesive character of the regolith material.

Measurements by the PROP instrument, which was part of the Lunokhod 1 payload, showed that the bearing capacity of the regolith along the traverse varied from 0.04 to 1.44 kg/cm^2, with a modal value close to 0.45 kg/cm^2. The shear strength of the regolith material was found to be between 0.02 and 0.1 kg/cm^2, with a modal value close to 0.05 kg/cm^2 (Leonovich et al., 1978). Accuracies of these measurements are estimated to be 5–10% of the measured values (Malenkov, personal communication). Values of these two parameters were found to decrease by a factor of 3–4 with an increase of the surface slope from ~2 to 12°. Similar values of the regolith bearing capacity and its dependence on surface slope were found for the regolith of the Lunokhod 2 study area in northeast Mare Serenitatis within the mare-flooded Le Monnier Crater (Basilevsky et al., 1984).

The chemical composition of the regolith material was measured by the X-ray-fluorescence spectrometer “RIFMA” (Kocharov and Viktorov, 1978). Although this instrument made measurements at almost every traverse station, measurements of sufficient duration to provide good statistics of the data were made at only four stations. The following chemical compositions were measured at four stations (recalculated in mass % of oxides): SiO_2–36.4 to 51.4%, FeO–10.3 to 16.7%, CaO–8.4 to 12.6%, Al_2O_3–11.3 to 18.9%, TiO_2- < 6.7%, K_2O- < 1.2–2.4%. If we consider the overall range of compositions these values correspond marginally to low-Ti aluminous basalts (Taylor et al., 1991). If we consider compositions measured at individual stations the closest although still marginal is the correspondence to low-Ti aluminous basalts observed at station 10 about 250 m north of the Luna 17 landing site.

3. Chang'E-3 area

The Chang'E-3 lander, with the Yutu rover onboard, landed in the northwestern part of Mare Imbrium in between craters Laplace F and Le Verrier E, ~500 km NE of the Luna17/Lunokhod 1 landing site (Fig. 1). The Chang'E-3 landing site coordinates are 44.12°N, 19.51°W (Xiao et al., 2015). According to analysis of remote sensing data, the landing site is within the Eratosthenian lava unit near the boundary with older Imbrian-aged lavas (Zhao et al., 2014; Wu et al., 2015). The Yutu rover was safely delivered to the lunar surface and started to traverse, making scientific observations with its stereo cameras, ground penetrating radar and spectrometers. The total length of the Chang'E-3 route is ~114 m. Fig. 12 shows the lander imaged by the panoramic camera of the rover.

CE3_BMYK_PCAML-C-004_SCI_N_20140113190347_20140113190347_0008_A;

CE3_BMYK_PCAML-C-005_SCI_N_20140113190450_20140113190450_0008_A

The Chang'E-3 spacecraft landed on the lunar surface on the east rim of a crater ~450 m in diameter (named Crater C1 in Xiao et al., 2015). At the final stage of landing it used terrain recognition equipment and software to hover ~100 m above the surface and confirm if it was safe for landing. Fig. 13 shows the landing site on the images taken by LRO NAC and the Chang'E-3 descent camera.

Yutu is a six-wheel rover with a mass of 140 kg. Its wheel width is 15 cm (http://wiki.china.org.cn/wiki/index.php/Yutu_%28Jade_Rabbit%29) and as in the case with Lunokhod 1 panoramas, the tracks of Yutu seen in panoramas are a convenient tool to measure sizes and distances. Yutu explored the lunar surface and subsurface on the rim of Crater C1 using its four main instruments: panoramic camera, Lunar Penetrating Radar (LPR), Visible-Near Infrared Spectrometer (VNIS), and Active Particle-Induced X-ray Spectrometer (APXS).

3.1. Craters

It is seen in Fig. 13a that the Crater C1 is morphologically prominent. It has inner slopes with maximum steepness ~20–25° and a depth-diameter ratio close to 1/6. This corresponds to the

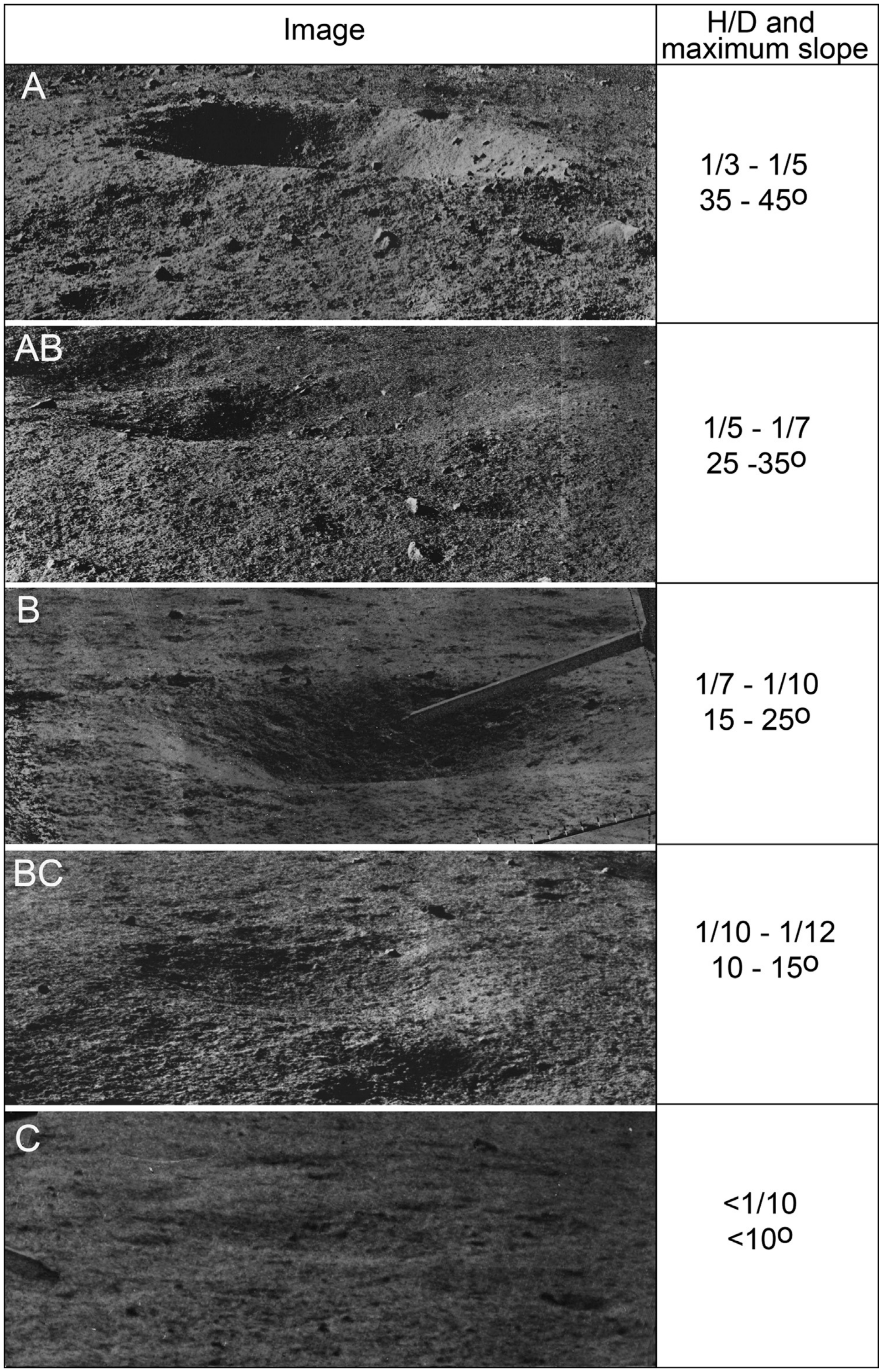

Fig. 7. Morphologic classification of small lunar craters. The craters shown are 3–5 m in diameter. Portions of Lunokhod 1 panoramas L1_D08_S03_P05, L1_D10_S03_P04, L1_D09_S02_P03, L1_D03_S07_P15 (flipped horizontally), L1_D_032_S04_P25 (flipped horizontally), correspondingly. In the right part of figure the typical depth/diameter ratios and maximum angles of crater internal slopes are shown.

transition from morphologic class AB to class B (Lu et al., 2014) and allows one to estimate the age of this crater as ~100 Ma (Basilevsky, 1976). Xiao et al. (2015) studied the crater size-frequency distribution within the Crater C1 rim, counting craters on LROC NAC image M181302794L, and determined the model age of ~27 Ma (see for details their Figure S8). So the Chang'E-3 landing area is geologically very young and the local soil here should be immature and rocky (McKay et al., 1991). This can be seen in Fig. 13b: the 17-m-diameter crater ~17 m north of the lander designated by Xiao et al. (2015) as Crater C2 has a rocky rim. Its depth of excavation is only about 1.5 m; on the basis of the crater radius and distance from the crater center, the Crater C1 ejecta thickness is calculated to be about 4–6 m (McGetchin et al., 1973, formula 3; Basilevsky et al., 1983, formula II.34). Similar estimates

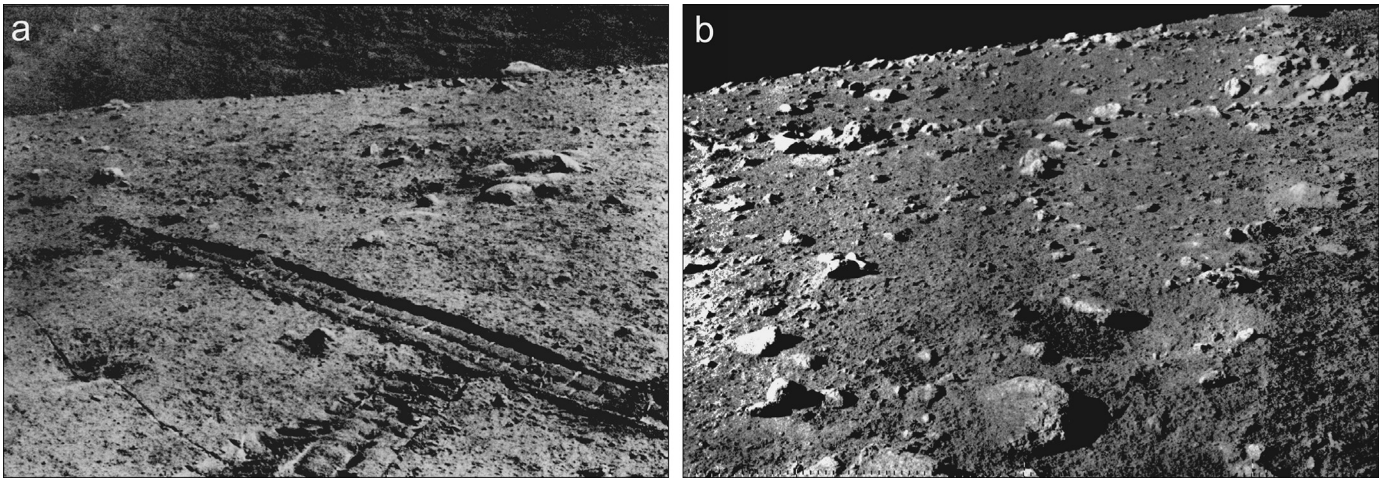

Fig. 8. (a) Moderately rocky surface in the WSW part of the rim of the relatively large (D=470 m) crater Borya (see Fig. 3). In the upper part of the image the opposite internal slope of this crater is seen. (b) Rocky surface on the western internal slope of crater Borya. Parts of panoramas L1_D07_S04_P08 and L1_D06_S02_P03, correspondingly.

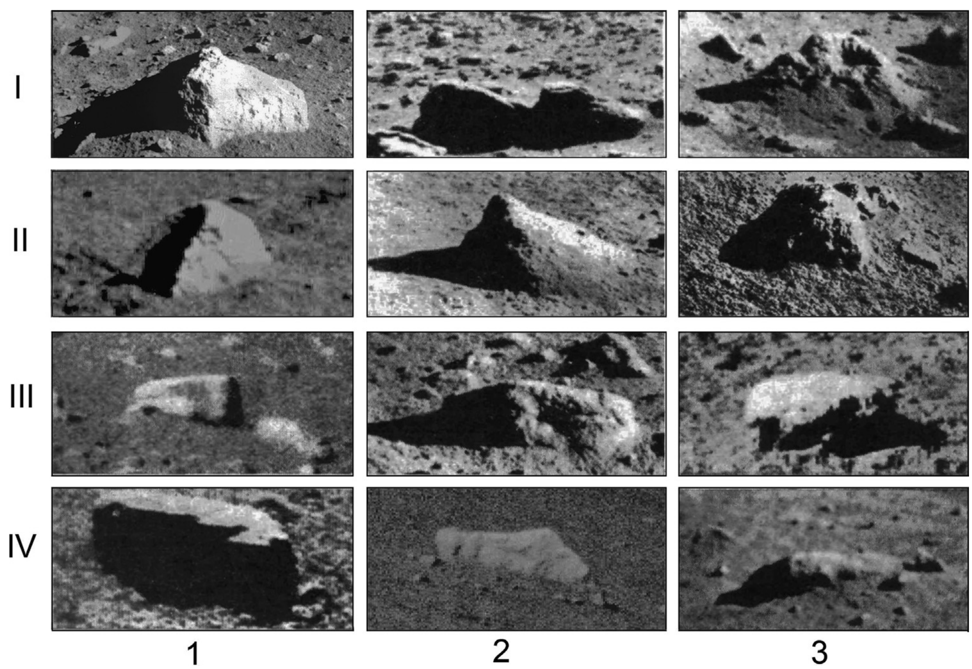

Fig. 9. Lunokhod 1 rover images of rock shapes and degrees of degradation. I–IV–The rock shape: irregular, pyramidal, prismatic and flattened, correspondingly. 1–3–Degree of degradation: angular, rounded-angular, rounded, correspondingly. The rocks shown are 30 cm to ~1 m in diameter. Parts of Lunokhod 1 panoramas.

made by Qiao et al. (2015) derived a thickness of 5 m. On this basis, it appears that Crater C2 did not penetrate below the blocky ejecta of Crater C1 and excavated mostly these ejecta.

The view of the southern part of Crater C1 and the crater eastern rim taken by the Yutu rover camera can be seen in Fig. 14.

CE3_BMYK_PCAML-C-014_SCI_N_20140113191411_20140113191411_0008_A;

CE3_BMYK_PCAML-C-015_SCI_N_20140113191514_20140113191514_0008_A

In Fig. 14 it is seen that the rim of Crater C1 is covered by numerous rock fragments, typically a few decimeters across. The largest rock in the lander near vicinity is the so called Loong Rock, 1.5 × 4 m (see below; Xiao et al., 2015). But it is seen in this figure and in Fig. 12 that generally the meter-sized rock blocks are present on inner slopes of the Crater C1, but practically absent on its rim where they certainly were emplaced at the time of crater formation, however then with time were destroyed. This suggests, according to Basilevsky et al. (2013), that crater C1 is ~100 Ma old, and this is in agreement with other age estimates based on crater morphologic prominence and size (Abdrakhimov et al., 2014; Lu et al., 2014), as previously discussed.

In close proximity to the landing site, a number of craters with sizes of decimeters to meters, and 15–20 m in diameter, are seen, with various degree of maturity (Fig. 15).

3.2. Rock fragments

Rock fragments in the Chang'E-3 study area, as in the Lunokhod 1 area, are mostly associated with fresh craters. Their highest abundance in the Chang'E-3 study area is observed within the

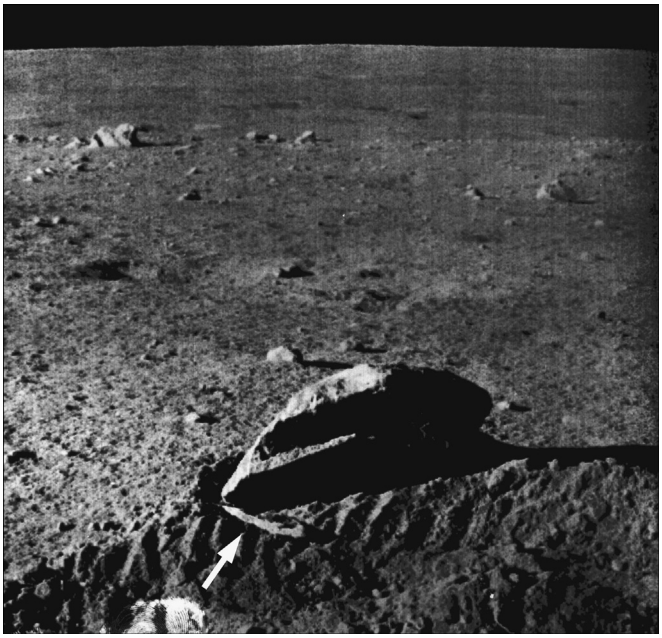

Fig. 10. A rock fragment, whose shape suggests that the source rock was characterized by columnar jointing. Part of panorama L1_D05_S01_P01.

rimcrest and inner slopes of the Crater C1 (D ≈ 450 m, morphologic prominence transitional from class AB to class B). Rock fragments here, as in the Lunokhod 1 area, vary in primary shape and degree of degradation, as summarized in Fig. 16. The varieties of rock fragments seen in this figure appear very similar to those observed in Fig. 9 in Lunokhod 1 images.

CE3_BMYK_PCAML-C-018_SCI_N_20140113191821_20140113191821_0008_A

CE3_BMYK_PCAML-C-015_SCI_N_20140113191514_20140113191514_0008_A

CE3_BMYK_PCAML-C-024_SCI_N_20140113192435_20140113192435_0008_A

CE3_BMYK_PCAML-C-009_SCI_N_20140113190859_20140113190859_0008_A

CE3_BMYK_PCAML-C-016_SCI_N_20140113191616_20140113191616_0008_A

CE3_BMYK_PCAML-C-009_SCI_N_20140113190859_20140113190859_0008_A

CE3_BMYK_PCAML-C-009_SCI_N_20140113190859_20140113190859_0008_A

CE3_BMYK_PCAML-C-006_SCI_N_20140113190552_20140113190552_0008_A

CE3_BMYK_PCAML-C-018_SCI_N_20140113191821_20140113191821_0008_A

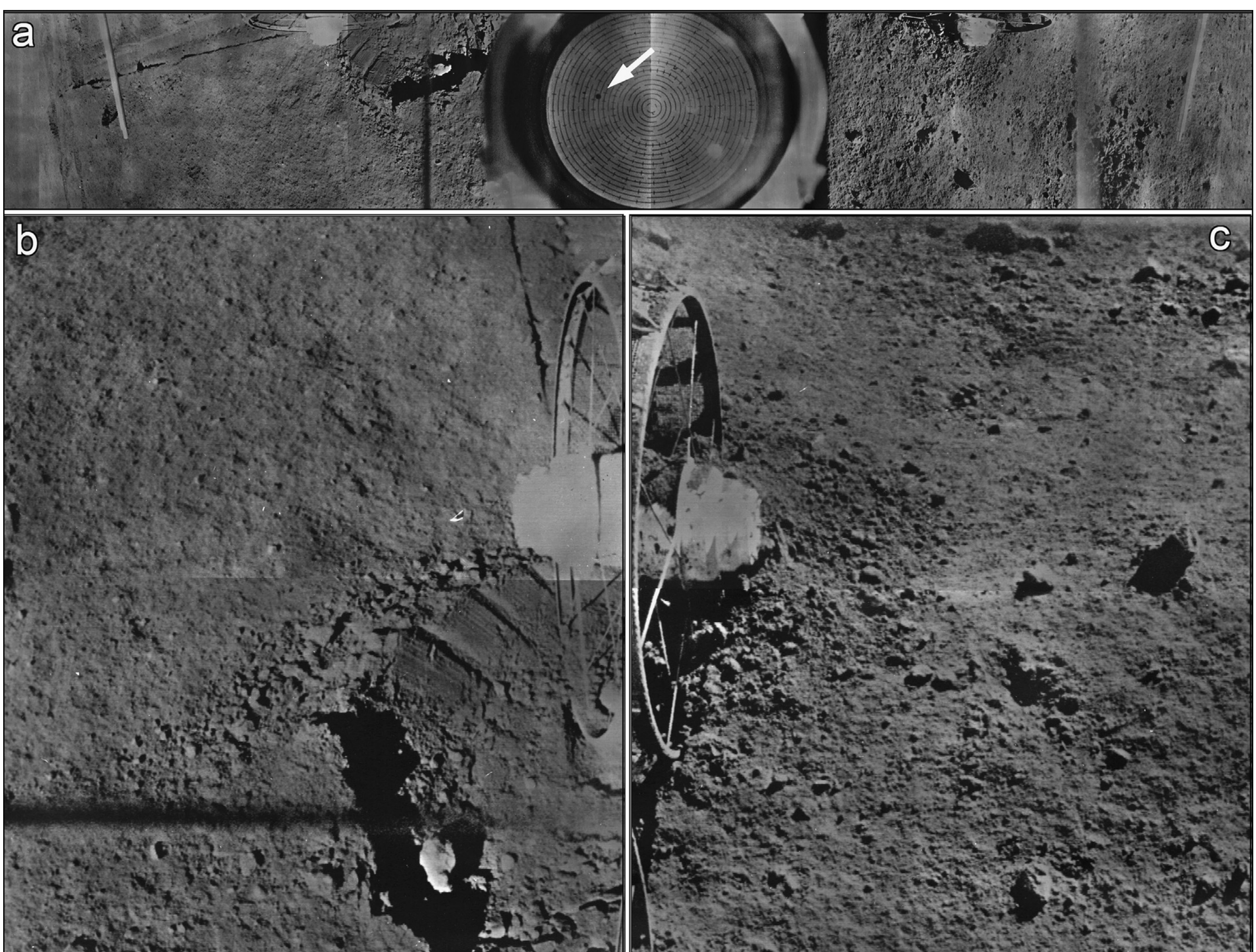

Fig. 11. (a) Panorama L1_D1_S04_P10 taken by the camera with horizontal axis of scanning. Its left part shows the lunar surface behind the rover, the right part, the surface ahead, and the central part shows a device to measure roll and pitch of the camera: the bowl with a graduated surface on which a small ball (white arrow) moves to different positions at different rolls and pitches. (b) and (c) the left and right parts of the panorama enlarged and turned clockwise and counterclockwise, correspondingly.

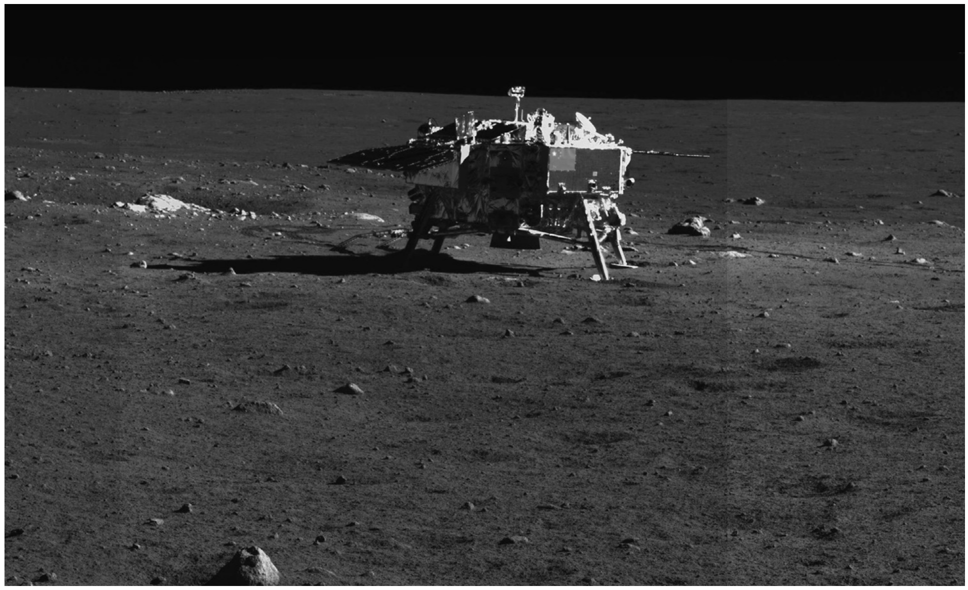

Fig. 12. Chang'E-3 lander on the lunar surface. For scale: the diagonal distance between the lander feet is 4.76 m. Portion of Yutu panorama, images.

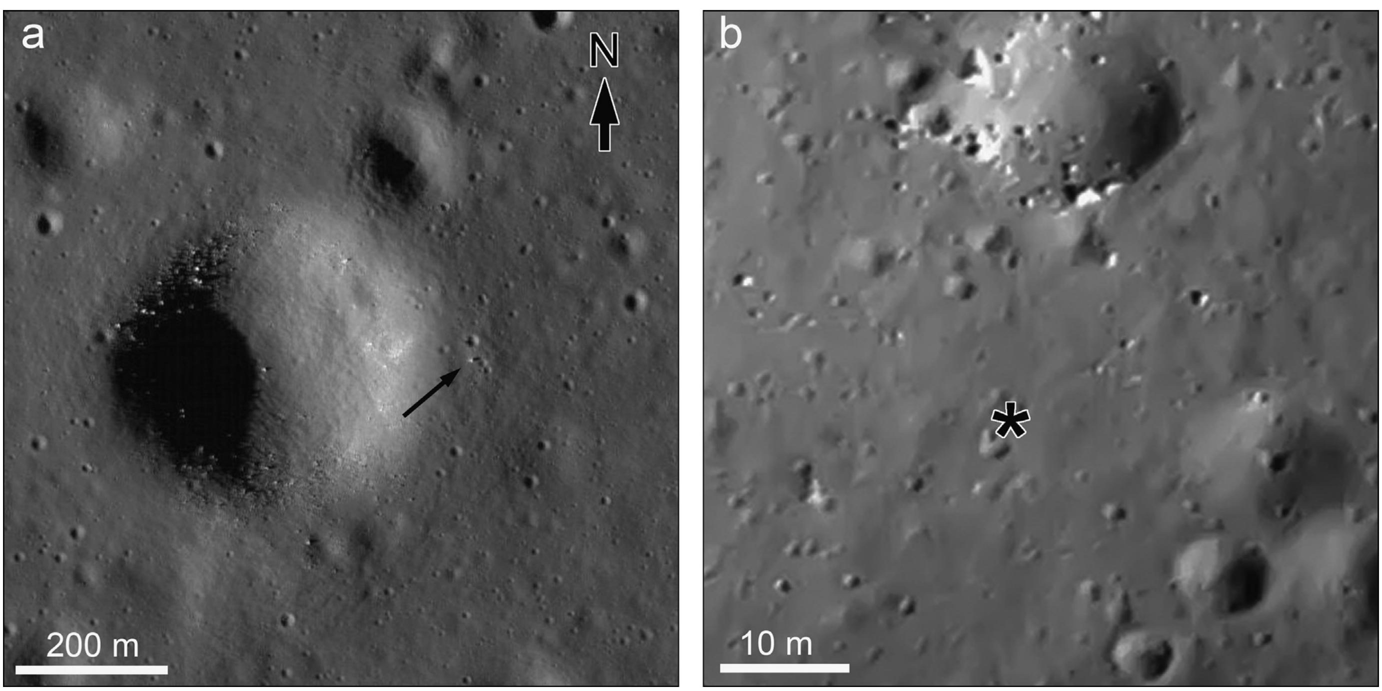

Fig. 13. Crater C1. (a) Portion of LRO NAC image M1142582775R showing the 450 m crater with Chang'E-3 lander seen (at end of black arrow) on its eastern rim. The image was taken on December 25, 2013, nine days after the landing. (b) Portion of image 4′57″ taken by the Chang'E-3 descent camera 4 min and 57 s from the beginning of the video showing the immediate vicinity of the landing site (http://www.youtube.com/watch?v=QzZkF1MAsb8). Asterisk denotes the final lander locality.

CE3_BMYK_PCAML-C-037_SCI_N_20131224193949_20131224193949_0006_A
CE3_BMYK_PCAML-C-009_SCI_N_20140113190859_20140113190859_0008_A
CE3_BMYK_PCAML-C-019_SCI_N_20140113191923_20140113191923_0008_A

Among the observed rocks, one rock fragment appears to represent an example of columnar jointing (Fig. 17). Comparing its size and angular distance from the rover with those for the lander and the rover wheel tracks seen in different part of the same panorama, it was possible to estimate that the rock is ~1 m long and 15 cm wide. The rock is observed on the rim crest of the 450-m Crater C1; this suggests that it was ejected from a depth of ~40–50 m, while its sharp-edged appearing pristine morphology probably indicates that for significant part of the time since formation of Crater C1 this rock was in the subsurface and only recently was excavated by a small impact cratering event (compare with Fig. 10 in the Lunokhod 1 part and the related text there). A few similar-appearing elongated rocks are seen at greater distances on the western inner slope of Crater C1.

The largest rock that Yutu rover approached is Loong Rock, ~1.5 m high and 4 m long. It consists of a few closely adjacent parts, the larger of which is shown in Fig. 18a.

The Loong Rock is described by Xiao (2014) and Xiao et al. (2015) as coarse-grained rock, basalt or dolerite, with brighter millimeter-sized inclusions, probably phenocrysts. Besides the

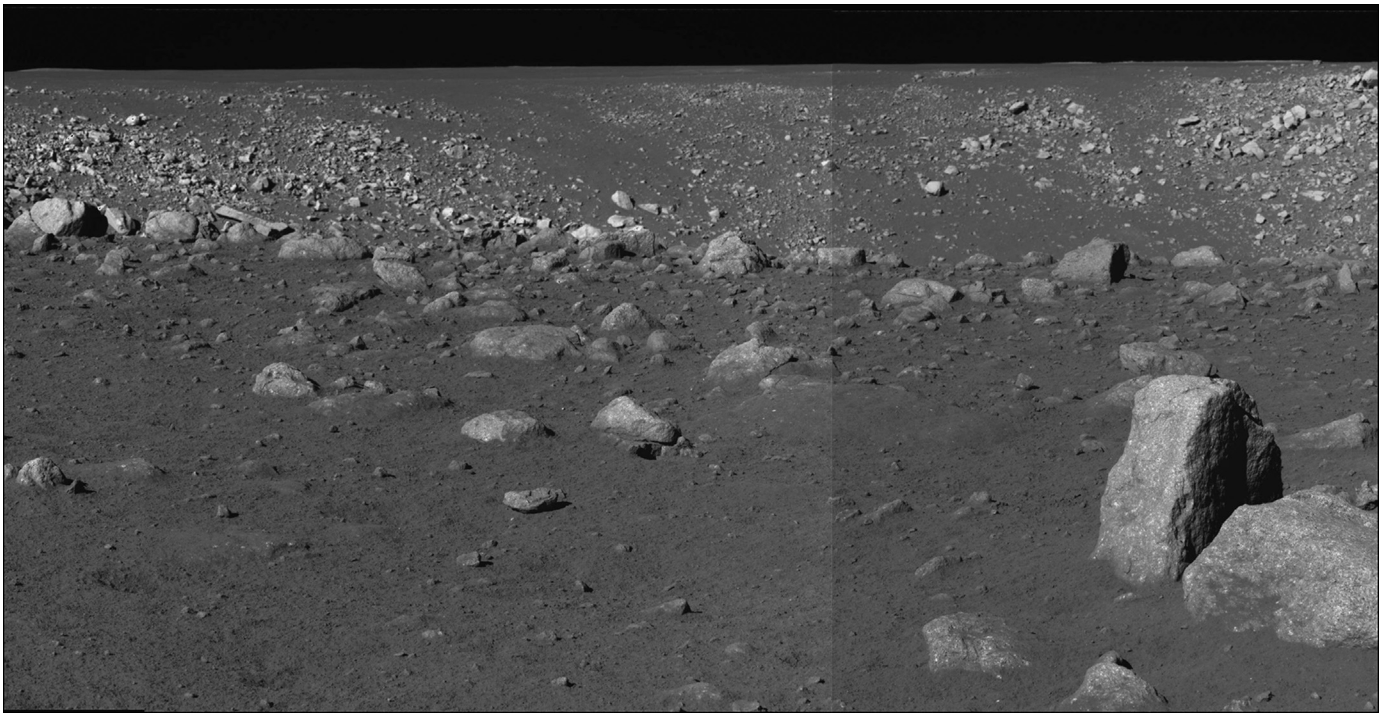

Fig. 14. Crater C1. Southeastern part of the rim (foreground) and southwestern part of inner crater wall slopes (background). The "standing" prismatic rock fragment in the lower right of the figure is ~0.5 m high. Portion of Yutu panorama, images.

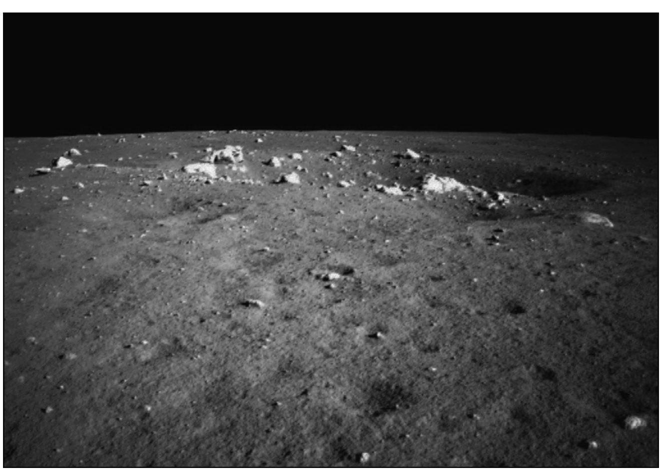

Fig. 15. The morphologically prominent crater C2 of 17 m in diameter (see also Fig. 13) and smaller craters of various morphologic prominence. Portion of Yutu panorama, part of image 074 from http://moon.bao.ac.cn/multimedia/img2dce3.jsp.

phenocrysts, also seen on the surface of this rock are microcraters (Fig. 18b), similar in appearance to those seen on the surface of the returned Apollo samples, for example Apollo 15 sample 15555, composed of basalt (Fig. 18c). The Loong Rock is estimated to have been exposed on the surface since the formation of Crater C1 (~100 Ma, see above) and rock sample15555 was exposed on the surface for approximately the same time: 76–90 Ma (Marti and Lightner, 1972; Podosek et al., 1972; York et al., 1972).

3.3. Regolith

The surface of the regolith at the Chang'E-3 site, as it is seen in Figs. 12, 14 and 15, can be both rocky and smooth. The regolith physico-mechanical properties were not measured here but as it can be concluded from the images of the wheel tracks (Fig. 19), they are probably rather similar to those at the Lunokhod 1 site (Figs. 2, 6, 8).

It is seen in Fig. 19 that the wheel tracks of the Yutu rover and Lunokhod 1 look rather similar. Considering the different masses of the Yutu rover (140 kg) and Lunokhod 1 (756 kg), the number of wheels (6 and 8) and the wheel diameter (30 and 50 cm) and wheel width (15 cm and 20 cm) one can conclude that the wheel load on the soil in case of Yutu differs from that of Lunokhod 1 by less than a factor of 2.5. This suggests that the strength of the upper part of regolith in these two localities probably does not differ much.

Qiao et al. (2015) studied small crater morphologies and their frequencies of distribution within the broad vicinity (5×5 km) of the Chang'E-3 site and found that the average regolith thickness here is 5–7 m; this is in agreement with estimations by Fa et al. (2014) and Shkuratov and Bondarenko (2001).

The Yutu rover was equipped with ground penetrating radar which sounded the subsurface structure of the regolith along the whole Yutu traverse (Qiao et al., 2015; Su et al., 2014; Xiao et al., 2015; Zhang et al., 2015). The instrument has two dominant frequencies: 60 MHz (Channel 1, which revealed subsurface structures to depths of ~400 m) and 500 MHz (Channel 2, which revealed structures at depths less than 12 m, but with greater detail compared with the Channel 1 data). It was found that the upper layer, which is a regolith formed after the Crater C1 crater-forming event, is 1–2 m thick. Below this, down to the depth of ~4 m, is the layer representing ejecta of Crater C1. Underlying the ejecta is a layer, whose base is at a depth of 6–10 m, interpreted as regolith accumulated before the formation of Crater C1. Materials at depths larger than ~6–10 m show regular layering and the radar echoes indicate a higher density compared with shallower regolith or ejecta deposits. This competent material extending to the depth of 35 m is considered to be the Eratosthenian basalts. Below this is a several meters thick layer interpreted as paleoregolith formed on top of the Imbrian-aged lava flows; within the Imbrian flows are

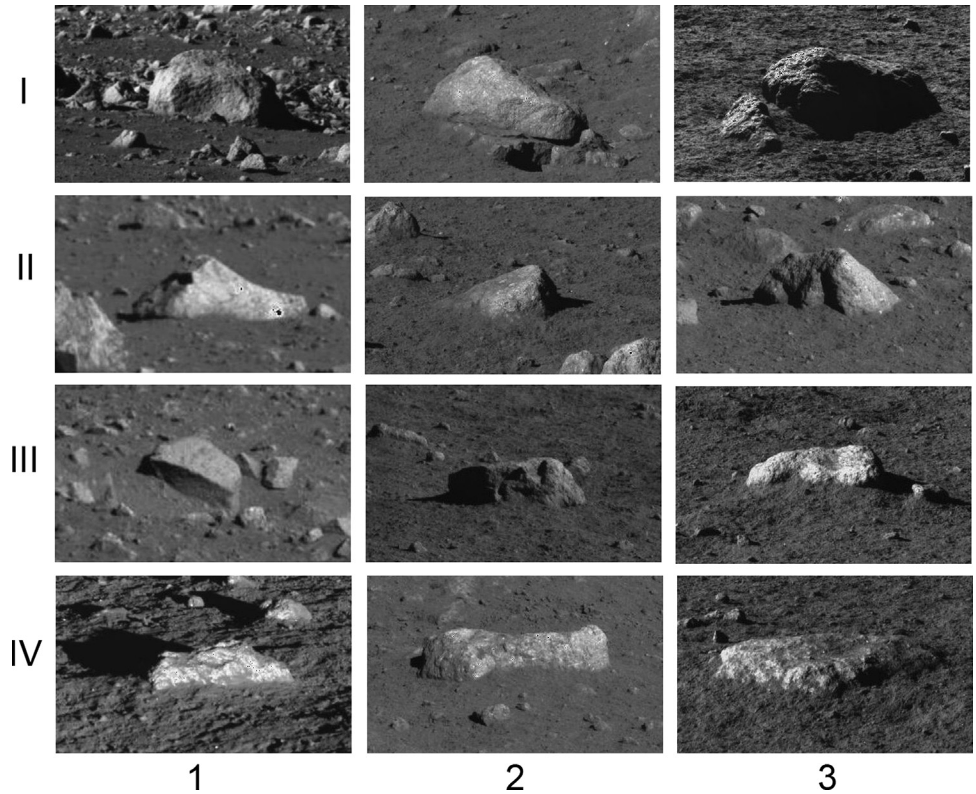

Fig. 16. Yutu rover images of rock shapes and degrees of degradation. I–IV–Rock shape: irregular, pyramidal, prismatic and flattened, correspondingly. 1–3-Degree of degradation: angular, rounded-angular, rounded, correspondingly. Compare to those seen in the Lunokhod 1 traverse panoramas (Fig. 9). The rocks shown are a few decimeters in diameter. Parts of the Yutu panoramas (from I to IV and left to right).

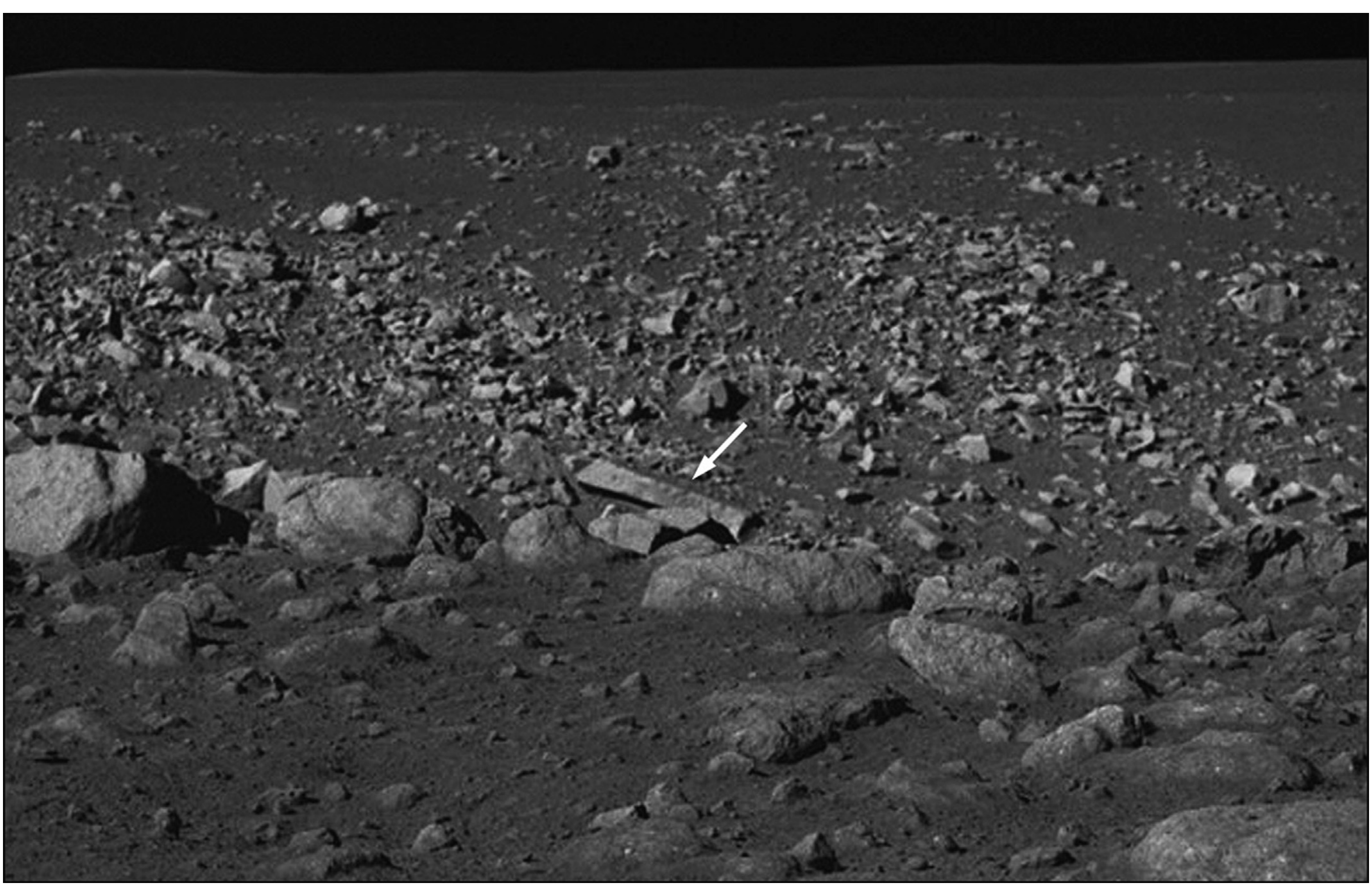

Fig. 17. Columnar fragment (arrow) on the rim of Crater C1. Portion of Yutu panorama, part of image ID: CE3_BMYK_PCAML-C-015_SCI_N_20140113191514_20140113191514_0008_A.

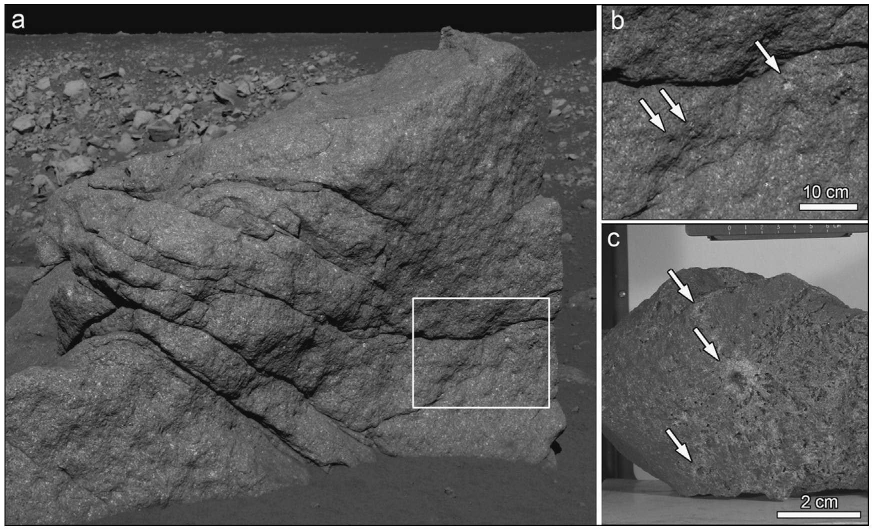

Fig. 18. (a) The major part of Loong Rock; (b) enlargement of the area outlined by box in (a), arrows point to microcraters a few millimeters in diameter; (c) the Apollo 15 rock sample 15555, arrows point to microcraters. Figure parts (a) and (b) are portions of image CE3_BMYK_PCAML-C-015_SCI_N_20140113191514_20140113191514_0008_A; (c) is part of NASA image S71-43393 (http://www.lpi.usra.edu/lunar/samples/atlas/).

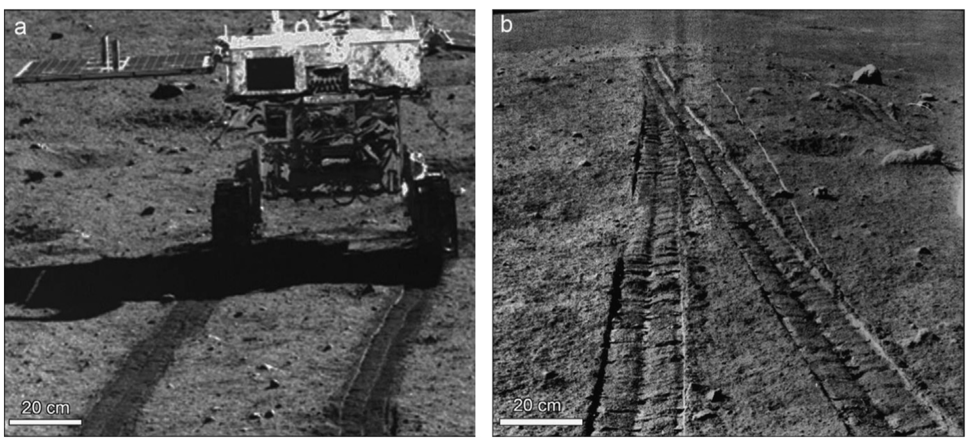

Fig. 19. Wheel tracks of Yutu rover (a) and Lunokhod 1 (b). Parts of the Chang'E-3 lander panorama portion of image 043 from http://moon.bao.ac.cn/multimedia/img2dce3.jsp and Lunokhod 1 panorama L1_D02_S05_P20. Scale bars are for the close parts of the images.

seen boundaries at depths of 140, 240 and 360 m. Zhang et al. (2015) report different depths at which these boundaries are seen: 195, 215, and 345 m.

The Visible-Near Infrared Spectrometer (VNIS) instrument made measurements in four points along the Yutu route (Liu et al., 2014; Zhang et al., 2015). The measurements covered ~20 × 20 cm surface areas at a distance of ~1.3 m in front of the rover. The spectral range was from 450 nm to 2400 nm. The spectra clearly document the presence of high-Ca pyroxene and are consistent with basalts. The presence of abundant olivine is also suggested but is more difficult to quantify. Additional data are needed for more detailed interpretations.

The Active Particle-Induced X-ray Spectrometer (APXS) operated at three points along the Yutu traverse (Neal et al., 2015). The measurements showed that regolith here contains approximately 4.7 wt% TiO_2, 12–12.6 wt% Al_2O_3, 21.3–22.1 wt% FeO, 8.3–9.1 wt% MgO, ~10.1 wt% CaO, and ~0.12 wt% K_2O. When compared with results taken by Clementine, Lunar Prospector and Chang'E-1 orbital data (Lucey et al. 2000; Prettyman et al., 2006; Wu et al., 2012) it was found that discrepancies evident between orbital and CE-3 data are only in TiO_2 (lower than orbital) and FeO (higher than orbital). Neal et al. (2015) considered the possibility of additions of highlands material to the local regolith or dilution of local material by low-Ti basaltic material from spatially close localities of the latter, and rejected these options, concluding that the CE-3 XRS data represent a new type of mare basalt. Zhang et al. (2015), considering contents of KREEP-indicative trace elements, supports the idea of a new type of basalt and suggests two different scenarios as to how it could be formed. The obvious differences in the spatial resolution of the measurements compared (centimeters versus hundreds of meters) should also be taken into account.

4. Discussion

As described above, the Luna 17/Lunokhod 1 site and Chang'E-3/Yutu site are very similar in surface geology. The major landforms are small impact craters, ranging from decimeters to a few hundred meters in diameter, and displaying various degrees of morphologic degradation. Rock fragments typically associated with morphologically fresh craters, and mostly occurring on the crater rims and internal slopes, are observed in both sites. Rock shapes, and degrees of rock morphologic degradation, are similar at the two sites. Sporadic rock fragments implying the presence of columnar jointing in the source rocks were found at both the

Lunokhod 1 and Chang'E-3 sites. They were observed on the rims of craters 450–470 m in diameter, suggesting that these rock fragments originated from the depths of 40–50 m.

The regolith in both regions explored is locally rather fine-grained, and locally rocky. The mean thickness of the regolith layer in the Lunokhod 1 and Chang'E-3 areas was estimated to be ~4–6 m, but on the rims and floors of the largest craters it may reach a few tens of meters. The Yutu ground penetrating radar found that the regolith structure and thickness along its 114 m traverse (Xiao et al., 2015). The three-unit structure of regolith was found here: the upper 1–2 m thick layer of regolith formed due to impact regardening of the Crater C1 ejecta, the middle 2–3 m thick layer of unreworked Crater C1 ejecta and the lower 4–6 m thick layer formed before emplacement of Crater C1. Evidence was found for the presence of one more layer of several meters thickness, interpreted as regolith material occurring between the layers of Eratosthenian and Imbrian-aged lavas at depths of 30–50 m (paleoregolith). On the basis of the Yutu ground-penetraing radar results (Xiao et al., 2015), it is clear that different varieties of multilayered regolith structure should have also occurred in the Lunokhod 1 area, and in majority of other mare areas as well.

The similarity in appearance of the Yutu and Lunokhod 1 wheel tracks suggests a similarity in the surface material strength as measured in the Lunokhod 1 area (bearing capacity from 0.04 to 1.44 kg/cm^2 with a modal value ~0.45 kg/cm^2: shear strength from 0.02 to 0.1 kg/cm^2 with modal value ~0.05 kg/cm^2, both decreasing by factor 3–4 with increase of the surface slope from 2 to 12°). On the basis of the Lunokhod measurements and the Yutu images, these values are probably typical of the Yutu traverse region as well.

The regolith chemical compositions measured in the Lunokhod 1 and Yutu sites raise questions because they differ from those derived from the remote sensing data for the Eratosthenian-aged basalts on which these two sites are located. The Lunokhod 1 measurements showed values of Si, Fe, Ca, Al, Ti, and K (Kocharov and Viktorov, 1978) which correspond marginally to low-Ti aluminous basalts (Taylor et al., 1991). The Yutu measurements showed difference from the orbital remote sensing data in TiO_2 (lower than orbital) and FeO (higher than orbital). On the basis of the Yutu measurements, Neal et al. (2015) suggested that the surface material here could derive from a new type of mare basalt and this suggestion is in agreement with the conclusions of Zhang et al. (2015). Part of the orbital/in-situ data discrepancy could be due to low measurement accuracies, especially in the case of Lunokhod 1. But the discrepancies may also be due to real variations in the composition of the surface materials, especially at the small spatial scale. The classification of the four major known types of lunar basalts are derived from the limited number of the sites from which sample were returned, and thus, mare basalt petrologic variability may be higher than is currently envisioned (e.g., Taylor et al., 1991).

5. Conclusions

- Luna 17/Lunokhod 1 and Chang'E-3/Yutu sites are both within the Eratosthenian-aged mare lava flow geologic unit and analysis of the in-situ data gained by these rovers showed that the geology of these sites is very similar, thus emphasizing that even over widespread areas of the same unit, characteristics of emplacement and regolith formation can be similar.
- As in the majority of other lunar places the dominant landforms in these sites are small impact craters having various degrees of morphologic prominence, and rock fragments, the latter mostly associated with rims and interiors of fresh craters. Rock shape and degree of preservation of the observed rock fragments in these two sites are rather similar.
- In both the Lunokhod 1 and Yutu sites sporadic rock fragments were observed whose morphologies suggest that their source rocks were characterized by columnar jointing. Localization of these specific rocks on the rims of craters of 450–470 m in diameter implies that the source rocks were derived from depths of 40–50 m.
- Regolith in the study areas is typically a few meters thick. The ground penetrating radar of the Yutu rover showed the multi-layer nature of the regolith structure, which is obviously determined by superposition of crater ejecta and which, with some variations, should be typical of the majority of other lunar mare sites.
- The physico-mechanical properties of regolith in these two sites seem to be rather similar: bearing capacity from 0.04 to 1.44 kg/cm^2 with modal value ~0.45 kg/cm^2 and the shear strength from 0.02 to 0.1 kg/cm^2 with modal value ~0.05 kg/cm^2, both decreasing by a factor of 3–4 with an increase of surface slope from 2 to 12°.
- The chemical composition of surface materials determined by the rover instruments at these two sites differ from those derived from the remote sensing data for the Eratosthenian-aged basalts on which these two sites are located. This could be partly due to low measurement accuracies, especially in the case of Lunokhod 1, but may also represent real variations in the composition of the surface materials compared to returned lunar samples.

6. Suggestions for future exploration

Lunokhod 1 (1970) was the first robotic lunar rover and initiated the era of mobile planetary research laboratories. Yutu is the most recent robotic lunar rover and the 43 year time interval between these two missions could provide, and in some respects did provide, a basis for improvements. Modern technologies made it possible to decrease the total mass of the rover by more than a factor of 5 (140 kg vs. 756 kg), maintaining approximately the same number of scientific instruments onboard (4 vs. 6). The smaller mass of the rover requires smaller launchers, and this makes missions less expensive and thus more economically plausible.

Panoramic cameras of Yutu compared to those of Lunokhod 1 are of smaller mass and provided higher resolutions and color capability. The Active Particle-Induced X-ray Spectrometer (APXS) of Yutu compared to the X-ray Fluorescence Spectrometer RIFMA on Lunokhod 1 is also of smaller mass and provided higher accuracies of elemental composition measurements. Yutu did not have an instrument to measure the physico-mechanical properties of the soil, like Lunokhod's PROP. This required the use of the visual appearance of the wheel tracks of Yutu for indirect estimates (see above). But Yutu did have ground penetrating radar which is an innovation in in-situ planetary research that provided valuable knowledge on the details of subsurface structure. This instrument should be recommended for future robotic rovers because in most study sites the subsurface structure is deduced based on general geological considerations, but these should be quantitatively tested and calibrated.

Yutu has a robotic arm with the APXS spectrometer mounted on it and this provided the possibility to move the instrument to the target of measurement. RIFMA was on the main body of the Lunokhod 1 rover, being only 30 cm above the lunar surface and could measure the surface composition of some area in the close vicinity (decimeters) ahead of the rover (Kocharov et al., 1971). Theoretically RIFMA could measure compositions of low rocks, but it was not in the field of view of the TV cameras so it was always a risk to damage it in the case of a collision with a rock. In reality, only soil surfaces were measured. Thus, the robotic arm of the Yutu rover is a valuable tool, which should be recommended for future lunar (and other planetary) rovers.

Robotic arms proved their effectiveness in the Mars Exploration Rovers and Curiosity missions (e.g., Arvidson et al., 2006; Squyres et al., 2006; Grotzinger et al., 2014). In the case of future lunar rover(s) the robotic arms could bear a microscopic imager, various spectrometers and a tool to clean up dusty surfaces. In a precursor or in a companion mission of sample return, the robotic arm should have the ability to pick up various samples. After the Lunokhod 2 mission there were serious discussions in the Soviet space research community about sending to the Moon a rover that would collect samples which would then be delivered to Earth by a companion spacecraft landing in the vicinity of the sample-collecting rover, guided by a radiobeacon on that rover.

A rover with a robotic arm operating as a companion for the sample return mission could take samples at different radial distances from the rims of relatively large craters. It is well known from cratering mechanics (e.g., Basilevsky et al., 1983; Melosh, 1989) that the deepest target materials are deposited as ejecta on the crater rim and with increasingly outward distance, materials of shallower horizons are deposited. In the case of crater Borya at the Lunokhod 1 area or Crater C1 at the Chang'E-3 site, this could be a way to study the stratigraphy down to a depth of 40–50 m. If the site in this, or in the precursor mission(s), was studied with ground penetrating radar, the subsurface structure determined can be compared with the sample sequence. Of course, such crater-associated radial studies make sense not only in the case of sample return but for in-situ studies as well.

This short discussion shows that by considering what was done by both the Lunokhod 1 and Yutu rovers, important improvements in strategy and tactics of future studies can be suggested. Two instruments/devices (ground penetrating radar and robotic arm) and crater-associated radial studies are strongly recommended for future missions.

Acknowledgments

We thank Russian Academy of Sciences/Roskosmos and the five systems in the Chinese Lunar Exploration Project and National Astronomical Observatories of Chinese Academy of Sciences (NAOC) for providing the Lunokhod 1 and Chang'E-3/Yutu data. We acknowledge NASA Lunar Reconnaissance Orbiter (LRO) Mission, Lunar Orbiter Laser Altimeter (LOLA) Experiment Team (Grants NNX11AK29G and NNX13AO77G), and NASA Solar System Exploration Research Virtual Institute (SSERVI) grant for Evolution and Environment of Exploration Destinations under cooperative agreement number NNA14AB01A at Brown University for ATB, CMP and JWH. This research was supported by the National Natural Science Foundation of China (41422110). Discussions with M.I. Malenkov, one of the key members of the Lunokhod chassis and PROP instrument teams, were very helpful. We acknowledge the reviewers for helpful comments.

References

Abdrakhimov, A.M., Basilevsky, A.T., Head, J.W., 2014. Local geologic setting along the Lunokod 1 traverse as analog for characteristics of the Chang'E-3 landing site. In: Proceedings of the 45th Lunar and Planetary Science Conference. Abs. #1239.

Anisov, K.S., Mastakov, V.I., Ivanov, O.G., et al., 1971. General design and assembling of Luna 17 spacecraft. In: Vinogradov, A.P. (Ed.), Mobile Laboratory on the Moon Lunokhod-1. Nauka Press, Moscow, pp. 7–20, in Russian.

Arvidson, R.E., Squyres, S.W., Anderson, R.C., et al., 2006. Overview of the spirit Mars exploration Rover mission to Gusev Crater: landing site to Backstay Rock in the Columbia Hills. J. Geophys. Res. 111 (E2), CiteID E02S0.

Basilevsky, A.T., 1974. Age of small lunar craters. Izvestiya AN SSSR, Ser. Geo. 8, 139–142, in Russian.

Basilevsky, A.T., 1976. On the evolution rate of small lunar craters. In: Proceedings of the 7th Lunar Science Conference. Pergamon Press, New-York, pp. 1005–1020.

Basilevsky, A.T., Grebennik, N.N., Gromov, V.V., Dmitriev, F.D., Kemurdzhian, A.L., Polosukhin, V.P., Semenov, P.S., Florensky, C.P., 1984. Dependence of physico-mechanical properties of lunar soil on characteristics of relief and processes in the study area of Lunokhod-2. Kosm. Issled. XXII (2), 243–251, in Russian.

Basilevsky, A.T., Head, J.W., Horz, F., 2013. Survival times of meter-sized boulders on the surface of the Moon. Planet. Space Sci. 89, 118–126.

Basilevsky, A.T., Ivanov, B.A., Florenskii, K.P., Yakovlev, O.I., Fel'dman, V.I., Granovskii, L.B., 1983. Impact Craters on the Moon and Planets. Nauka Press, Moscow, p. 200, in Russian.

Basilevsky, A.T., Kreslavsky, M.A., Karachevtseva, I.P., Gusakova, E.N., 2014. Morphometry of small impact craters in the Lunokhod-1 and Lunokhod-2 study areas. Planet. Space Sci. 92, 77–87.

Fa, W., Liu, T., Zhu, M.-H., Haruyama, J., 2014. Regolith thickness over Sinus Iridum: results from morphology and size-frequency distribution of small impact craters. J. Geophys. Res. 119 (E8), 1914–1935.

Florensky, C.P., Basilevsky, A.T., Pronin, A.A., Popova, Z.V., 1971. Preliminary results of geomorphological analysis of panoramas. In: Vinogradov, A.P. (Ed.), Mobile Laboratory on the Moon Lunokhod-1. Nauka Press, Moscow, pp. 96–115, in Russian.

Florensky, C.P., Basilevsky, A.T., Gurshtein, A.A., Zasetsky, V.V., Zezin, R.B., Pronin, A. A., Popova, Z.V., 1972. Geomorphological analysis of the area of Mare Imbrium explored by the automatic roving vehicle Lunokhod 1. Space Research XII. Akademie-Verlag, Berlin, pp. 107–121.

Florensky, C.P., Basilevsky, A.T., Ivanov, A.V., 1977. Role of exogenic factors in the formation of the lunar surface. In: The Soviet-American Conference on Geochemistry of the Moon and Planets. NASA SP-370. Washington, D.C., pp. 571–584.

Florensky, C.P., Basilevsky, A.T., Zezin, R.B., Polosukhin, V.P., Popova, Z.V., 1978. Geologic-morphologic studies of lunar surface. In: Barsukov, V.L. (Ed.), Mobile Laboratory on the Moon Lunokhod-1, 2. Nauka Press, Moscow, pp. 102–135, in Russian.

Florensky, C.P., Taborko, I.M., 1972. Some conclusions on the morphometry of the areas of the Moon photographed by Luna-12 probe. In: Physics of the Moon and Planets, Nauka Press, Moscow, pp. 150–153. in Russian.

Grotzinger, J.P., Sumner, D.Y., Kah, L.C., et al., 2014. A habitable fluvio-lacustrine environment at Yellowknife Bay, Gale Crater, Mars. Science 343 (6169), id. 1242777.

Hiesinger, H., Head, J.W., Wolf, U., Jaumann, R., Neukum, G., 2010. Ages and stratigraphy of lunar mare basalts in Mare Frigoris and other nearside maria based on crater size frequency distribution measurements. J. Geophys. Res: Planets 115, E03003.

Ivanov, O.G., Ryvkina, V.A., Nepoklonov, B.V., 1978. Work of Lunokhod 1 on the Moon in February–September 1971. In: Barsukov, V.L. (Ed.), Mobile Laboratory on the Moon Lunokhod-1, 2. Nauka Press, Moscow, pp. 7–24, in Russian.

Karachevtseva, I., Oberst, J., Scholten, F., et al., 2013. Cartography of the Lunokhod-1 landing site and traverse from LRO image and stereotopographic data. Planet. Space Sci. 85, 175–187.

Kocharov, G.E., Borodulin, N.F., Viktorov, S.V., Voropaev, O.M., Dzevanovskaya, A.Yu, Ivanov, O.G., Kiryan, G.V., Petrov, V.V., Sakulskiy, V.A., 1971. Lunar automatic spectrometric instrument RIFMA. In: Vinogradov, A.P. (Ed.), Mobile Laboratory on the Moon Lunokhod-1. Nauka Press, Moscow, pp. 89–95, in Russian.

Kocharov, G.E., Viktorov, S.V., 1978. Study of chemical composition of lunar soil by Lunokhod 1. In: Barsukov, V.L. (Ed.), Mobile Laboratory on the Moon Lunokhod-1, 2. Nauka Press, Moscow, pp. 92–101, in Russian.

Leonovich, A.K., Ivanov, O.G., Pavlov, P.S., et al., 1978. Automotive chassis of Lunokhod 1 as instrument for the lunar surface study. In: Barsukov, V.L. (Ed.), Mobile Laboratory on the Moon Lunokhod-1, 2. Nauka Press, Moscow, pp. 25–43, in Russian.

Liu, B., Li, C.L., Zhang, G.L., et al., 2014. Data processing and preliminary results of the Chang'E-3 VIS/NIR Imaging Spectrometer in-situ analysis. Res. Astron. Astrophys. 1 (12), 1578–1594.

Lu, Y., Basilevsky, A. and Abdrakhimov, A., 2014. Local geology of Chang'E-3 landing site from analysis of the CE-3 descent camera and LROC NAC images. In: Proceedings of the 45th Lunar and Planetary Science Conference. Abs. #1116.

Lucey, P.G., Blewet, D.T., Jolliff, B.L., 2000. Lunar iron and titanium abundance algorithms based on final processing of Clementine ultraviolet-visible images. J. Geophys. Res. 105 (E8), 20,297–20,305.

Marti, K., Lightner, B.D., 1972. Rare gas record in the largest Apollo 15 rock. Science 175, 421–422.

McGetchin, T.R., Settle, M., Head, J.W., 1973. Radial thickness variation in impact crater ejecta: implications for lunar basin deposits. Earth Planet. Sci. Lett. 20, 226–236.

McKay, D.S., Heiken, G., Basu, A., Blanford, G., Simon, S., Reedy, R., French, B.M., Papike J., 1991. The lunar regolith. In: Lunar Source Book: A User Guide to the Moon. Cambridge University Press, New-York, pp. 285–357.

Melosh, H.J., 1989. Impact Cratering: A Geologic Process. Oxford University Press, New York, p. 245.

Morris, E.S., Shoemaker, E.M., 1968. Fragmental debris. In: Surveyor Project Final Report. NASA Technical Report 32-1265. Washington, D.C., pp. 69–86.

Neal, C.R., Wu, Y.Z., Cui, X.Z., Peng, W.X., Ping, J.S., 2015. Regolith at the Chang'E-3 landing site: a new type of mare basalt composition. In: Proceedings of the 46th Lunar and Planetary Science Conference. Abs. #1641.

Qiao, L., Xiao, L., Zhao, J., Huang, Q., Haruyama, J., 2014. Geological features and evolution history of Sinus Iridum, the Moon. Planet. Space Sci. 101, 37–52.

Qiao, L., Xiao, Z.Y., Zhao, J.N., Xiao, L., 2015. Subsurface structures at the Chang'E-3 landing site: interpretations from orbital and in-situ imagery data. In: Proceedings of the 46th Lunar and Planetary Science Conference. Abs. #1050.

Podosek, F.A., Huneke, J.C., Wasserburg, G.J., 1972. Gas retention and cosmic ray exposure ages of lunar rock 15555. Science 175, 423–425.

Prettyman, T.H., Hagerty, J.J., Elphic, R.C., Feldman, W.C., Lawrence, D.J., McKinney, G.W., Vaniman, D.T., 2006. Elemental composition of the lunar surface: analysis of gamma ray spectroscopy data from Lunar Prospector. J. Geophys. Research. 111, E12007.

Schultz, P.H., 1976. Moon Morphology. University of Texas Press, Austin and London, p. 626.

Schaber, G.G., 1969. Geologic map of the Sinus Iridum quadrangle of the Moon, US Geological Survey. IMAP 602. U.S. Geological Survey, Washington, D.C.

Schaber, G.G., 1973. Lava flows in Mare Imbrium: Geologic evaluation from Apollo orbital photography. Geochim. Cosmochim. Acta 1, 73–92.

Shingareva, K.B., Karachevtseva, I.P., Dovgan, V.G., Basilevsky, A.T., Baskakova, M.A., Gusakova, E.N., 2012. Lunokhod-1 traverse map (Landing site Luna-17). MIIGAiK, DLR, Moscow ⟨http://planetology.ru/panoramas/Lunokhod-1_traverse_map_Luna_17.pdf⟩.

Shkuratov, Yu.G., Bondarenko, N.V., 2001. Regolith layer thickness mapping of the Moon by radar and optical data. Icarus 149, 329–338.

Squyres, S.W., Arvidson, R.E., Bollen, D., et al., 2006. Overview of the opportunity Mars exploration Rover mission to Meridiani Planum: eagle crater to Purgatory Ripple. J. Geophys. Res. 111 (E12), CiteID E12S12.

Su, Y., Fang, G.Y., Feng, J.Q., et al., 2014. Data processing and initial results of Chang'E-3 lunar penetrating radar. Res. Astron. Astrophys. 14 (12), 1623–1632.

G.J. Taylor P. Warren G. Ryder J. Delano C. Pieters G. Lofgren Lunar rocks. In Lunar Source Book: A User Guide to the Moon 1991 Cambridge University Press New-York 183 284.

Wilhelms, D.E., 1987. The Geologic History of the Moon. U.S. Geological Survey Professional Paper 1348. Washingnon, D.C., pp. 302, 12 plates.

Wu, Y., Head, J.W., Pieters, C.M., Basilevsky, A.T., Li, L., Li, F., Chen, L., Luo, X., Lu, Y., Chen, Y., 2015. Compositional diversity and geologic context of the northwest Imbrium region. (in preparation).

Wu, Y., Xue, B., Zhao, B., Lucey, P., Chen, J., Xu, X., Li, C., Ouyang, Z., 2012. Global estimates of lunar iron and titanium contents from the Chang'E-1 IIM data. J. Geophys. Res. 117, E02001.

Xiao, L., 2014. China's touch on the Moon. Nat. Geosci. 7, 391–392.

Xiao, L., Zhu, P., Fang, G., et al., 2015. A young multilayered terraine of the northern Mare Imbrium revealed by Chang'E-3 mission. Science 347 (6227), 1226–1229.

York, D., Kenyon, W.J., Doyle, R.J., 1972. 40Ar−39Ar ages of Apollo 14 and 15 samples. In: Proceedings of the 3rd Lunar Science Conference. pp. 1613–1622.

Zhang, J., Yang, W., Hu, S., et al., 2015. Volcanic history of the Imbrium basin: a close-up view from the lunar rover Yutu. Proc. Natl. Acad. Sci. 112 (17), 5342–5347.

Zhao, J.N., Huang, J., Qiao, L., Xiao, Z.Y., Huang, Q., Wang, J., He, Q., Xiao, L., 2014. Geologic characteristics of the Chang'E-3 exploration region. Sci. China–Phys., Mech. Astron. 57, 569–576. http://dx.doi.org/10.1007/s11433-014-5399-z.